

Lancemaside A from *Codonopsis lanceolata* is a broad-spectrum antiviral agent against SARS-CoV-2 and variants of concern

TAI YOUNG KIM¹, Sangeun Jeon², Meehyun Ko², Young Eun Du³, So-Ri Son³, Dae Sik Jang³, Seungtaek Kim², and Changjoon Justin Lee¹

¹Institute for Basic Science

²Institut Pasteur Korea

³Kyung Hee University

September 1, 2022

Abstract

Background and Purpose *Codonopsis lanceolata* (CL) has long been used as a medicinal herb in East Asian countries to treat inflammatory diseases of the respiratory system but its antiviral activity has not been investigated. Here, we evaluated the potential inhibitory activity of CL extracts and their active compounds on SARS-CoV-2. **Experimental Approach** Pseudotyped SARS-CoV-2 entry assay and dose-response curve analysis with authentic SARS-CoV-2 and recombinant SARS-CoV-2 reporter virus expressing the nanoluciferase were carried out to investigate the effects of compounds against SARS-CoV-2 entry into host cells. Filipin cholesterol staining, SARS-CoV-2 Spike (S)-ACE2 binding assay, and S-mediated cell fusion assay using time-lapse imaging, flow cytometry, and split-GFP fusion were conducted to understand the inhibitory mechanisms. **Key Results** Lancemaside A (LA), a triterpenoid saponin isolated from CL, impeded the endosomal entry pathway of SARS-CoV-2 and its variants including Alpha, Beta, Delta, and Omicron with similar IC₅₀ values of 2.23 ~ 3.37 μ M as well as the TMPRSS2-mediated viral entry pathway with IC₅₀ value of 3.92 μ M. LA was also able to prevent the formation of S-induced multinucleated syncytia. Mechanically, LA altered the distribution of host cell membrane cholesterol and blocked the membrane fusion between SARS-CoV-2 and host cells. **Conclusion and implications** LA can be a broad-spectrum antiviral drug not only against SARS-CoV-2 but also against other novel enveloped viral pathogens that might arise in the future by targeting viral envelope fusion with the host cell membrane. **Keywords** SARS-CoV-2, Omicron, COVID-19, Lancemaside A, triterpenoid saponin, membrane fusion

Lancemaside A from *Codonopsis lanceolata* is a broad-spectrum antiviral agent against SARS-CoV-2 and variants of concern

Tai Young Kim^{1*}, Sangeun Jeon^{2*}, Meehyun Ko², Young Eun Du³, So-Ri Son⁴, Dae Sik Jang^{3,4}, Seungtaek Kim², C Justin Lee¹

¹ Center for Cognition and Sociality, Institute for Basic Science, Daejeon 34126, Korea.

² Zoonotic Virus Laboratory, Institut Pasteur Korea, Seongnam, Korea.

³Department of Life and Nanopharmaceutical Sciences, Graduate School, Kyung Hee University, Seoul 02447, Korea.

⁴Department of Biomedical and Pharmaceutical Sciences, Graduate School, Kyung Hee University, Seoul 02447, Korea

e-mail: dsjang@khu.ac.kr; seungtaek.kim@ip-korea.org; cjl@ibs.re.kr

* These authors equally contributed to this work.

Background and Purpose

Codonopsis lanceolata (CL) has long been used as a medicinal herb in East Asian countries to treat inflammatory diseases of the respiratory system but its antiviral activity has not been investigated. Here, we evaluated the potential inhibitory activity of CL extracts and their active compounds on SARS-CoV-2.

Experimental Approach

Pseudotyped SARS-CoV-2 entry assay and dose-response curve analysis with authentic SARS-CoV-2 and recombinant SARS-CoV-2 reporter virus expressing the nanoluciferase were carried out to investigate the effects of compounds against SARS-CoV-2 entry into host cells. Filipin cholesterol staining, SARS-CoV-2 Spike (S)-ACE2 binding assay, and S-mediated cell fusion assay using time-lapse imaging, flow cytometry, and split-GFP fusion were conducted to understand the inhibitory mechanisms.

Key Results

Lancemaside A (LA), a triterpenoid saponin isolated from CL, impeded the endosomal entry pathway of SARS-CoV-2 and its variants including Alpha, Beta, Delta, and Omicron with similar IC_{50} values of 2.23 ~ 3.37 μ M as well as the TMPRSS2-mediated viral entry pathway with IC_{50} value of 3.92 μ M. LA was also able to prevent the formation of S-induced multinucleated syncytia. Mechanically, LA altered the distribution of host cell membrane cholesterol and blocked the membrane fusion between SARS-CoV-2 and host cells.

Conclusion and implications

LA can be a broad-spectrum antiviral drug not only against SARS-CoV-2 but also against other novel enveloped viral pathogens that might arise in the future by targeting viral envelope fusion with the host cell membrane.

Keywords

SARS-CoV-2, Omicron, COVID-19, Lancemaside A, triterpenoid saponin, membrane fusion

Introduction

During the ongoing coronavirus disease 2019 (COVID-19) pandemic, five variants of concern (VOCs) of the severe acute respiratory syndrome coronavirus 2 (SARS-CoV-2) have been identified (Scovino, Dahab, Vieira, Freire-de-Lima, Freire-de-Lima & Morrot, 2022). Alpha variant (lineage B.1.1.7) was first detected in the United Kingdom in early 2020 and then four additional variants including Beta (B.1.351), Gamma (P.1), Delta (B.1.617.2), and Omicron (B.1.1.529) have emerged and spread to many countries (Aleem, Akbar Samad & Slenker, 2022). Omicron, first reported to the World Health Organization (WHO) from South Africa on November 24, 2021, now has overtaken the previous variants and became the dominant variant around the world (Gowrisankar, Priyanka & Banerjee, 2022; Rahmani & Rezaei, 2022). Changes of dominant variant over time have been attributed to enhanced transmissibility of newly emerging variant over previous ones due to the additional mutation on S protein and its increased affinity to human receptor protein ACE2 (Chen, Tsung-Ning Huang & Huang, 2022; Du et al., 2022). These S mutations also confer resistance to antibody-based therapeutics and evasion from infection- and/or vaccine-induced humoral immunity (Biswas et al., 2022; DeGrace et al., 2022; Hoffmann et al., 2022). Thus, therapeutic strategies targeting common mechanisms that contributes to the infection of SARS-CoV-2 and their variants are imperative.

The entry of SARS-CoV-2 into human cells requires the binding of viral envelope S protein to ACE2 cellular receptor and subsequent fusion between the viral and cellular membranes, releasing the viral genome in the cytoplasm (Hoffmann et al., 2020). The membrane fusion is mainly mediated by S protein that is comprised of two functional subunits termed S1 and S2, which are responsible for receptor binding and membrane fusion, respectively (Tang, Bidon, Jaimes, Whittaker & Daniel, 2020). Upon ACE2 binding, S protein undergoes a conformational change from pre-fusion conformation to a post-fusion structure via its proteolytic cleavage at S1/S2 sites by host cell proteases (Hoffmann et al., 2020). The hydrophobic fusion peptide (FP) of S2 subunit is exposed and inserted into host cell membranes, then the heptad repeat 1

(HR1) and 2 (HR2) domains in the S2 subunit are bound together to form a six-helix bundle (6-HB) fusion core, drawing the two membranes into close proximity to facilitate virus-cell fusion (Xia et al., 2020). Since the S2 subunit is highly conserved across the coronavirus family, FP and HR domains are considered as a key target for the development of pan-coronavirus fusion inhibitor (Huang, Yang, Xu, Xu & Liu, 2020; Xia et al., 2020). Previous studies have reported that HR2-derived peptides targeting the HR1 domain inhibit 6-HB formation, thereby blocking viral membrane fusion and cellular entry of human coronaviruses (Liu et al., 2004; Lu et al., 2014; Xia et al., 2019). It was also demonstrated that conjugation of cholesterol to the peptide sequence leads to the anchoring of the peptide to the cell membrane where fusion occurs, strongly potentiating its action (de Vries et al., 2021; Xia et al., 2020).

Natural products have been an important source of recent drug development (Newman & Cragg, 2020). Since the WHO declared COVID-19 as a pandemic, natural compounds have provided a wide array of potential anti-SARS-CoV-2 drug candidates with various cellular and viral targets. In line with this, we previously reported that platycodin D (PD), a natural component of *Platycodon grandiflorum* (PG), is capable of blocking SARS-CoV-2 infection (Kim et al., 2021). The roots of PG have been widely used to treat several respiratory diseases, such as asthma, airway inflammation, and sore throats (Choi, Hwang, Lee & Jeong, 2009; Lee et al., 2020). Similarly, the roots of *Codonopsis lanceolata* (CL) have been widely used as a traditional medicinal herb in East Asian country such as Korea, China, Japan for the treatment of several disorders including bronchitis, cough, and allergic lung inflammation (Hossen, Kim, Kim & Cho, 2016; Seo et al., 2019). It contains many biologically active compounds, including polyphenols, saponins, tannins, triterpene, alkaloids, and steroids (Du et al., 2018). But, whether CL extracts or their active compounds may have inhibitory activity against viruses including SARS-CoV-2 has not been investigated yet. In this study, we discovered that Lancemaside A (LA), a triterpenoid saponin isolated from CL, effectively inhibits the infection of SARS-CoV-2 and its variants including Alpha, Beta, Delta, and Omicron. We further found that LA affects the distribution of membrane cholesterol and blocks membrane fusion between SARS-CoV-2 and host cells to inhibit SARS-CoV-2 infection. These findings provide the first evidence that LA displays potent antiviral activity, particularly against SARS-CoV-2 and suggest the potential use of LA as a natural pan-coronavirus fusion inhibitor.

Methods

2.1 Plant Material

The aerial parts and roots of *Codonopsis lanceolata* Trautv. (Campanulaceae) used in this study were collected at Daemosan mountain, Seoul, Republic of Korea, in April, 2021. The origin of the plant was identified by D.S.J., one of authors, and voucher specimens (COLA-A-2021 and COLA-R-2021) has been deposited in the Laboratory of Natural Product Medicine, College of Pharmacy, Kyung Hee University, Seoul, Republic of Korea.

2.2 Extraction and Isolation

The fresh aerial parts (289 g) and roots (209 g) were sliced and extracted in an ultrasonic bath (room temperature for 2 hours with 3 L and 2 L of 70% EtOH, respectively) five times. The extracts were filtered and concentrated by a rotary evaporator to give 70% EtOH extracts of the aerial parts (29.4 g, 10.20%) and roots (23.5 g, 11.24%). The eight compounds tested in this study, tangshenoside I (1), ethylsyringin (2), syringin (3), sinapaldehyde glucoside (4), lobetyolin (5), lancemasides A (6), B (7), and D (8), were previously isolated from the roots of CL (Du et al., 2018).

2.3 Reagent

Echinocystic acid (purity, [?] \geq 95%) was purchased from Sigma-Aldrich Co. (USA).

2.4 Cells and viruses

H1299 cells were obtained from the Korean Cell Line Bank (KCLB, South Korea, 25803) and cultured in RPMI-1640 (Gibco, USA). HEK293T and Vero cells were obtained from the American Type Culture

Collection (CRL-3216 and CCL-81) and cultured in Dulbecco's Modified Eagle's Medium (DMEM; Corning, USA), respectively. Both culture media were supplemented with 10% fetal bovine serum (FBS) (Gibco, USA) and 1X Penicillin-Streptomycin solution (HyClone, USA). Cell cultures were incubated at 37°C in a humidified incubator containing 5% CO₂. For viruses, early isolates of SARS-CoV-2 viruses (NCCP43326) and four SARS-CoV-2 variants including Alpha (NCCP43381), Beta (NCCP43382), Delta (NCCP43390), and Omicron (NCCP43408) were obtained from Korea Disease Control and Prevention Agency (KDCA). These viruses were propagated in Vero E6 cells and the viral titers were determined by plaque assay using Vero cells. All experiments with these viruses were conducted in an enhanced biosafety level 3 (BSL-3) containment facility at Institut Pasteur Korea as approved by the KDCA.

2.5 Production of lentiviral particles and generation of stable cell lines

The full length SARS-CoV-2 spike sequence from SARS-CoV-2 spike plasmid (a gift from Fang Li, Addgene plasmid #145032) was cloned into pHR-CMV or pHR-CMV_IRES-EmGFP lentiviral expression plasmid (a gift from A. Radu Aricescu, Addgene plasmid #113887 and #113888) via EcoRI and AgeI restriction sites. Lentiviral plasmids encoding ACE2 and TMPRSS2 were cloned and obtained as described in previous work (Kim et al., 2021). For lentiviral packaging, HEK293T cells were co-transfected with the lentiviral expression plasmids and the packaging plasmid psPAX2 and envelope plasmid pMD2.G using Lipofectamine 3000 (Thermo Fisher, USA) according to the manufacturer's instructions. Supernatants containing the lentivirus were harvested at 24 h and 48 h post-transfection, combined, and filtered through 0.45 µm-pore-size filter. To generate stable cell lines, H1299 or HEK293T cells plated on a 6 well plate with 50-60% confluence were incubated with 1 ml of the viral supernatants in the presence of polybrene (Merck, Germany) at a final concentration of 4 µg/ml. After 24 h, the culture supernatants were changed with fresh medium and further cultured for an additional 2-3 days.

2.6 Production of SARS-CoV-2 S-pseudotyped lentivirus and pSARS-CoV-2 entry assay

SARS-CoV-2 S-pseudotyped lentiviruses (pSARS-CoV-2) was generated using 2th generation lentiviral packing system as described in previous work (Kim et al., 2021). Briefly, HEK293T cells that reached 70-80% confluency were transfected with lentiviral plasmid harboring a gene encoding for fly luciferase, psPAX2 packing plasmid, and SARS-CoV-2 S plasmid using Lipofectamine 3000 transfection reagent (Invitrogen, USA) following the manufacturer's instructions. At 24 h and 48 h post-transfection, culture supernatants containing pSARS-CoV-2 virus particles were collected and centrifuged at 500 × g for 5 min to remove the cellular debris, and stored at 4°C until use. For pSARS-CoV-2 entry assay, ACE2⁺ and ACE2/TMPRSS2⁺ H1299 cells plated on a 48 well plate with 60-80% confluency were pre-treated for 1 h with each drugs, followed by an overlay of supernatants containing pSARS-CoV-2 virus particles in the presence of each drugs. After 24 h incubation, viral entry efficiency was quantified by measuring the firefly luciferase activity in cell lysates using a luciferase assay system (Promega, USA) and SpectraMax iD5 Multi-Mode Microplate Reader (Molecular Devices, USA).

2.7 Dose-response curve (DRC) analysis by immunofluorescence assay

Vero cells were seeded at 1.2×10^4 cells per well in black, 384-well, µClear plates (Greiner Bio-One, Austria). After 24 h, the cells were transferred into the BSL-3 containment facility and SARS-CoV-2 was added at a multiplicity of infection (MOI) of 0.008 and incubated for additional 24 h. The cells were then fixed with 4% PFA and immunostained with an antibody against SARS-CoV-2 nucleocapsid (N) protein, and cell nuclei were visualized with DNA fluorochrome Hoechst 33342. The images were acquired using Operetta high-throughput imaging device (Perkin Elmer) and analyzed using Columbus software (PerkinElmer, Inc. Waltham, MA) to quantify cell numbers and infection ratios. Antiviral activity was normalized to infection control (0.5% DMSO) in each assay plate. DRCs were generated using Prism software (GraphPad). IC₅₀ values were measured in duplicates and calculated using nonlinear regression analysis.

2.8 Dose-response curve (DRC) analysis with SARS-CoV-2-Nluc

A549-ACE2-TMPRSS2 cells (1.2×10^4 cells per well) were plated into white 384-well µClear plates (Greiner

Bio-One). On the next day, the cells were treated with 2-fold serial dilution of the compound prepared in DMSO and infected with SARS-CoV-2-Nluc (MOI 0.01) (Rihn et al., 2021). After incubation at 37°C for 24 hours, nanoluciferase substrates (Promega) were added to each well and luciferase signals were measured using a VICTOR3™ multilabel plate reader (PerkinElmer). Cell viability was measured using the CellTiter-Glo Luminescent Cell Viability Assay (Promega, Madison, WI, USA) according to the manufacturer instructions. The relative luciferase signals of the compound-treated groups were normalized to that of non-infection control (set as 0%) and DMSO-treated groups (set as 100%). The DRCs were generated using Prism6 software (GraphPad, San Diego, CA), and IC₅₀ (half-maximal inhibitory concentration) and CC₅₀ (half-maximal cytotoxic concentration) values were calculated using a nonlinear regression model.

2.9 Cell viability assay

H1299 and Vero cells seeded in 96-well plate (5×10^3 cells/well) were treated with the indicated concentrations of CL extracts or each compounds for 24 h. Subsequently, WST-8 solution (Biomax, Korea) was added to each well and incubated for 2 h at 37°C in CO₂ incubator. The absorbance of the water-soluble formazan dye formed was measured at 450 nm using SpectraMax iD5 Multi-Mode Microplate Reader (Molecular Devices, USA). The relative cell viability was expressed as a percentage relative to the untreated control cells.

2.10 SARS-CoV-2 Spike-ACE2 binding assay

A recombinant protein containing receptor-binding domain (RBD) of the SARS-CoV2 spike protein fused with GFP (S-RBD-GFP) were produced in Expi293F cells after transfection of pcDNA3-SARS-CoV-2-S-RBD-sfGFP (a gift from Erik Procko, Addgene plasmid # 141184) using the ExpiFectamine 293 transfection kit and grown in Expi293 expression medium (Thermo Fisher Scientific, USA) for 4-5 days. The culture medium was cleared via centrifugation at 800xg for 5 min and stored at 4 degC until analysis. For the binding assay, ACE2⁺ H1299 cells were treated with DMSO or indicated concentrations of CL extracts or LA for 30 min, followed by incubation with a 1/10 dilution of medium containing S-RBD-GFP for 10 min at 37degC in CO₂ incubator. ACE2⁺ H1299 cells were then washed with PBS containing 1% BSA and analyzed for the binding of S-RBD-GFP using LSRFortessa flow cytometer (BD Biosciences). The data was analyzed using FlowJo software (BD Life Sciences).

2.11 S-mediated cell fusion assay using time-lapse microscopy and flow cytometry

For time-lapse microscopy, mRuby2 fluorescence-positive ACE2/TMPRSS2⁺ H1299 cells were seeded in clear bottom 24 well plates (ibidi, #82426;) overnight and then treated with DMSO or 10 μM LA for 1 h, followed by adding HEK293T cells expressing EGFP or both S protein and EGFP from a single bicistronic mRNA in (Spike-HEK293). Time-lapse fluorescence images were acquired at 4 min interval for 1 h at x40 magnification using Leica DMi8 microscope (Leica Microsystems, Germany). For flow cytometry assay, mRuby2-positivie ACE2/TMPRSS2⁺ H1299 cells were seeded in 12 well plate (2×10^5 cells/well) overnight and treated with DMSO, or 10 μM of lancemaside A, B, or D. After incubation for 30 min, 6.5×10^4 cells of EGFP-HEK293 or Spike-HEK293 cells were added and further incubated for 1 h at 37°C in CO₂ incubator. The co-cultures were harvested using trypsin-EDTA and 1×10^4 cells and analyzed by flow cytometry using LSRFortessa (BD Biosciences) to determine the percentage of EGFP and mRuby double-positive cells as a measure of heterologous cell fusion. The data was analyzed using FlowJo software (BD Life Sciences).

2.12 Split-GFP assay to detect the S-mediated syncytia formation

ACE2/TMPRSS2⁺ H1299 cells separately expressing two non-fluorescent fragments of GFP (GFP1-10 and GFP11)(Buchrieser et al., 2021) were established and equal numbers of these cells were plated in clear bottom 96 well plates (ibidi, #89626). Next day, the cultures were infected with lentiviral particles expressing SARS-CoV-2 S protein for 6 h and treated with DMSO or varying concentration of LA, followed by incubation for 36 h. The cells were then fixed with 4% paraformaldehyde (PFA) and stained with DAPI (Invitrogen, D1306) to identify the nuclei. Acquisition and automated analysis of the fluorescent cell images were carried out using an ImageXpress Pico system (Molecular Devices) with CellReporterXpress software (cell scoring function, 2 channel assay for scoring cells based on the DAPI stained nuclei and GFP images). Nuclei which

overlap with GFP fluorescence (designated as syncytia) and free nuclei were pseudocolored in green and red respectively using CellReporterXpress software and the percentage of syncytia formation was calculated as the ratio of green to (green + red) colored nuclei.

2.13 Filipin cholesterol staining

Cells grown on glass coverslips were fixed with 4% PFA and then stained with 5 $\mu\text{g}/\text{ml}$ filipin-III (Cayman, USA) in PBS containing 1% FBS for 2 h to examine intracellular distribution of free cholesterol. The stained cells were observed under a LSM 700 confocal microscope (Carl Zeiss, Germany). Signal intensities of plasma membrane were quantified using Image J software (<http://imagej.nih.gov/ij/>).

2.14 Western blot analysis

Protein samples from the cells of split-GFP assay (incubation time was prolonged to 72 h) were prepared by dissolving the cultures directly in 2X SDS sample buffer and analyzed by western blot analysis. The primary antibodies used were as follows; rabbit anti-cleaved caspase-3 and caspase-9 (Cell Signaling #9664 and #52873), and mouse anti-GAPDH (Abcam, ab8245). We used secondary antibodies conjugated with horseradish peroxidase (KPL, USA), and developed the blots using ECL Western Blotting Substrate (Thermo Fisher Scientific, USA). Images of original uncropped western blots were provided (Fig. S4).

2.15 Comparison of the infectivity of WT and D614G mutant of pSARS-CoV-2

To generate pSARS-CoV-2 harboring D614G mutation on spike protein, a single nucleotide A-to-G substitution was introduced by site-directed mutagenesis into SARS-CoV-2 spike plasmid using the primer sequence 5'-GTG GCC GTG CTG TAC CAG GGC GTG AAT TGC ACC GAG GTG -3'. WT and D614G pSARS-CoV2 viruses were produced as described above. The culture supernatants containing viral particles were filtered on 0.45 μm pore filter and concentrated by ultracentrifugation at 28,000 rpm for 2 h at 4°C in a Beckman SW28 rotor and an Optima XE-100 Ultracentrifuge (Beckman Coulter). The virus pellets were resuspended in PBS buffer and then viral titers were determined by qRT-PCR method using Lentivirus Titration Kit (LV900, ABM). The equivalent amount of WT and D614G pSARS-CoV2 viruses were used to infect host cells for pSARS-CoV-2 entry assay.

2.16 Statistical analysis

The data shown in this study are representative of two or three independent experiments and presented as the mean \pm SEM of triplicate samples. The results were analyzed using Student's t-test and a p value less than 0.05 was considered to indicate statistical significance (****P < 0.0001; NS not significant). Prism v.9.0.0 (GraphPad Software) was used for statistical analyses.

RESULTS

3.1 Triterpenoid saponins from *Codonopsis lanceolata* inhibit the infection of SARS-CoV-2

We first tested whether CL has an inhibitory activity against SARS-CoV-2 infection using a pseudovirus that expresses S protein on HIV-based lentiviral particles (pSARS-CoV-2), which has been used as a model system for analyzing SARS-CoV-2 infection (Crawford et al., 2020; Kim et al., 2021). pSARS-CoV-2 entry assay showed that the 70% EtOH extracts of the roots and aerial parts of CL prevented pSARS-CoV-2 from entering the ACE2-overexpressing H1299 human lung carcinoma cells (ACE2⁺ H1299) in a dose-dependent manner with half-maximal inhibitory concentrations (IC₅₀) of 251 $\mu\text{g}/\text{ml}$ and 540 $\mu\text{g}/\text{ml}$, respectively, without obvious cell toxicity (Figure. 1a and 1b). These results indicate that CL extracts contain substances with inhibitory activity against SARS-CoV-2 infection, which are higher in the roots than the aerial parts. In order to identify bioactive compounds in the CL, eight main compounds we previously isolated from the roots of CL (Du et al., 2018) were subjected to the examinations for their inhibitory effects against two SARS-CoV-2 entry pathways, that is, endosomal pathway in ACE2⁺ H1299 cells and TMPRSS2-mediated membrane fusion in ACE2 and TMPRSS2 double-positive cells (ACE2/TMPRSS2⁺ H1299) (Figure 1c). Our results revealed that both SARS-CoV-2 entry pathways were effectively blocked by pentacyclic triterpenoid saponins such as lancemaside A (LA) and lancemaside B (LB), but not others including lancemaside D (LD)

(Figure 1d), indicating that LA and LB are biologically active compounds responsible for the blockade of SARS-CoV-2 infection in CL extracts.

3.2 Lancemaside A inhibits two main SARS-CoV-2 entry pathways with a similar efficiency

Based on the results showing that LA has better inhibitory activity against SARS-CoV-2 than LB (Figure 1d), we chose LA for further experiments. First, we evaluated the ability of LA to inhibit pSARS-CoV-2 entry at various concentrations and obtained the IC_{50} values of 1.77 and 2.85 μM in ACE2⁺ and ACE2/TMPRSS2⁺ H1299 cells, respectively (Figure 2a and 2b). Notably, LA treatment in the range of concentrations did not induce cytotoxicity in H1299 cells (Figure 2c). We further extended our analysis to examine the effect of LA against the infection of authentic SARS-CoV-2 into Vero cells that express high levels of ACE2 but no detectable TMPRSS2 (Kim et al., 2021). Assessment of SARS-CoV-2 infection based on an immunostaining of SARS-CoV-2 nucleocapsid N protein in Vero cells showed that LA exhibited antiviral activity against ancestral SARS-CoV-2 with IC_{50} of 2.62 μM (Figure 2d). Importantly, LA was found to be more effective than remdesivir, an FDA-approved anti-SARS-CoV-2 drug (IC_{50} : 7.24 μM) (Figure 2e). We further verified the inhibitory activity of LA against TMPRSS2-dependent cell surface entry pathway of SARS-CoV-2 by measuring the infection of a recombinant SARS-CoV-2 reporter virus expressing the nanoluciferase (Nluc) (SARS-CoV-2-Nluc) into A549 cells that overexpress both ACE2 and TMPRSS2. The result showed that LA effectively blocked the viral entry in the cells with an IC_{50} of 3.92 μM (Figure 2f). Overall, these results demonstrate that LA restricts SARS-CoV-2 entry both at the endosomal compartments and at the cell surface

Lancemaside A inhibits SARS-CoV-2 entry by blocking S protein-mediated viral membrane fusion

Having observed that LA inhibits two main SARS-CoV-2 entry routes to similar extent, we reasoned that a possible target for LA could be a common step of both viral entry pathways. Therefore, we first examined the effect of LA on the interaction between SARS-CoV-2 spike (S) protein and ACE2. To do so, a recombinant protein containing receptor-binding domain (RBD) of the SARS-CoV-2 S protein fused with GFP (S-RBD-GFP) was produced and added into ACE2⁺ H1299 cells (Figure 3a). Flow cytometry showed that more than 97% of the cells were bound with S-RBD-GFP (Figure 3b), reflecting SARS-CoV-2 S attachment to cellular receptor for viral cell entry. Importantly, pretreatment of ACE2⁺ H1299 cells with CL root extracts or LA did not affect the binding of S-RBD-GFP to ACE2 on the cells within the effective concentration range we obtained in the anti-SARS-CoV-2 assays (Figure 1a and 2), despite somewhat inhibitory effects were seen at higher concentrations (Figure 3b). Moreover, LB, LD, and triterpenoid aglycone such as echinocystic acid (EA) did not display any inhibitory effects until their concentration reached 20 μM (Figure S1). Overall, these results suggest that S-ACE2 protein-protein interaction is not a main target for LA to inhibit SARS-CoV-2 infection. Thus, as a next step, we tested another possibility that LA may prevent fusion between the viral and host membranes, a process that commonly occurs in both entry pathways. For the assay, we established two stable cell lines: one that overexpresses S protein with EGFP from a single bicistronic mRNA in HEK293 cells (Spike-HEK293) and the other overexpressing mRuby in ACE2/TMPRSS2⁺ H1299 cells. Then, dual imaging time-lapse microscopy was performed to monitor cell fusion between these two cells as indicative of the S-mediated membrane fusion during viral entry (Figure S2). Addition of Spike-HEK293 cells to a monolayer of ACE2/TMPRSS2⁺ H1299 rapidly induced the cell-to-cell fusion, which allows them to fuse continuously with neighboring ACE2/TMPRSS2⁺ H1299 due to the S protein displayed on the surface of fused hybrid cells, eventually giving rise to enlarged multinucleated cells (Figure 3c). The heterologous cell fusion is mediated by the interaction between S protein and ACE2, because this process was not observed in co-culture of HEK293 expressing GFP only with ACE2/TMPRSS2⁺ H1299 cells (Figure 3c). We next examined the effects of LA on the cell-to-cell fusion event. Strikingly, LA treatment almost completely blocked the fusion of Spike-HEK293 cells with ACE2/TMPRSS2⁺ H1299 cells, implicating impairment of SARS-CoV-2 entry by LA at the membrane fusion step (Figure 3c). Furthermore, we quantified the cell-to-cell fusion by flow cytometry analysis after co-culturing the two cell types in a ratio 1 to 3. The results showed that approximately 30% of total cells were double-positive for mRuby and GFP, indicating

that most of Spike-HEK293 were participated in the fusion event (Figure 3d). Meanwhile, the double-positive cells were barely detected when control GFP-HEK293 cells (no S protein) were co-cultured with ACE2/TMPRSS2⁺ cells, again demonstrating the requirement of S protein during the cell-to-cell fusion (Figure 3d). Notably, LA pretreatment strongly blocked the fusion event, with less than 4 % of cells generating cell fusion hybrids (Figure 3d). On the other hand, LB and LD showed limited or no anti-fusion activity (Figure 3d), further supporting our results obtained in pSARS-CoV-2 entry assay (Figure 1d). Next, we investigated how LA may affect membrane fusion. We previously reported that PD, a triterpenoid saponin derived from PG, redistributes membrane cholesterol and inhibits SARS-CoV-2 infection (Kim et al., 2021). Membrane cholesterol is essential component for SARS-CoV-2 to gain entry into the host cells through membrane fusion (Sanders et al., 2021). As LA has a similar chemical structure to PD, we reasoned that LA might also alter membrane cholesterol content and undertook confocal microscopy analysis of filipin staining to investigate membrane cholesterol distribution after LA treatment. We found that 1 h treatment of ACE2⁺ H1299 cells with 10 μ M LA significantly led to an increase in cholesterol content at the plasma membrane and in endosomes (Figure 3e and 3f). Importantly, these redistributions of cholesterol were also observed upon treatment of parental H1299 cells with LA (Figure 3e and 3f), indicating that LA affects cell membrane directly, not by affecting ACE2. Moreover, we treated ACE2⁺ H1299 cells with LB, LD, and EA, and compared their effects on membrane cholesterol with that of LA. The cells showed that LB also increased the amount of cholesterol in plasma membrane by about 1.7-fold above DMSO-treated control, as revealed by filipin staining, but it was lower than that of LA (2.3-fold increase) (Figure S3). In addition, LD and EA did not show any effects on membrane cholesterol content (Figure S3). Intriguingly, the increased levels of membrane cholesterol caused by triterpenoid saponins from CL is well correlated with their inhibitory ability against S-mediated membrane fusion and viral infection (Figure 3d and Figure 1d), supporting the idea that membrane cholesterol might be a direct target for LA to exert its anti-SARS-CoV-2 activity. Taken together, our data suggest that LA interferes with the S-mediated membrane fusion, possibly by altering distribution of cholesterol on the host cell membrane, leading to inhibition of main SARS-CoV-2 infection routes.

Lancemaside A blocks syncytia formation Given that LA has an inhibitory activity for membrane fusion, we next sought to investigate the effects of LA on the formation of multinucleated giant cells called syncytia, which is a result of the continuous fusion of SARS-CoV-2-infected cells with neighboring cells and often detected in lung tissue from COVID-19 patients (Buchrieser et al., 2020; Bussani et al., 2020). For the assay, we employed a split-GFP complementation technology, in which half of GFP is expressed separately in different cells and a functional GFP protein can be reconstituted upon cell-to-cell fusion. ACE2/TMPRSS2⁺ H1299 cells stably expressing each of the two fragments of the reporter protein were generated and plated in equal number, and then S protein was ectopically expressed in these cell mixtures to induce syncytia formation, which can be detected by GFP fluorescence (Figure 4a and 4b). In DMSO-treated control cells, multiple enlarged GFP⁺ cells with clustered nuclei were detected, indicating syncytia were formed (Figure 4c, upper panel). Using automated image analysis, we quantified the efficiency of syncytia formation by dividing the number of nuclei in GFP⁺ multinucleated cells by the total number of nuclei in the field of view (Figure 4c, lower panel) and found that approximately 30% of the total number of cells plated formed GFP⁺ syncytia (Figure 4d). Importantly, the number of GFP⁺ cell clusters was dose-dependently reduced by LA treatment, with IC₅₀ values of 3.94 μ M, indicating that LA effectively inhibits the S-mediated syncytia formation (Figure 4c and 4d). As virus-induced syncytia formation generally promotes programmed cell death (Hooper, Zaki, Daniels & Middleton, 2001; Nardacci, Perfettini, Grieco, Thieffry, Kroemer & Piacentini, 2015), we next asked if LA is able to prevent the viral activation of apoptotic pathways. Consistent with previous studies, the S-mediated syncytia promoted apoptosis as evidenced by western blot analysis of the proteolytic cleavage of caspase 3 and 9 (Figure 4e). Notably, these apoptotic markers were not detected under no S expression and LA pretreatment conditions (Figure 4e). Together, these results indicate that LA blocks the S-induced syncytia formation and consequent apoptotic cell death.

LA effectively inhibits SARS-CoV-2 infection regardless of S mutation

Mutations in gene encoding S protein, which were found in most of SARS-CoV-2 variants, have been reported

to cause an increase in SARS-CoV-2 infectivity by enhancing attachment to ACE2 on the host cell surface (Ozono et al., 2021; Zaman, Orakzai & Yunus, 1987; Zhang et al., 2020). Among novel S mutations, D614G is the most common one found in the lineage B.1 of SARS-CoV-2 including Alpha, Beta, Delta, and Omicron variants (Schrors et al., 2021). To test whether LA can equally inhibit the enhanced SARS-CoV-2 infectivity mediated by S mutations, the D614G mutation was introduced into the S gene by site-directed mutagenesis. Consistent with previous studies, pSARS-CoV-2 carrying the D614G mutation showed a significantly higher infectivity compared to the wild type (WT) in both ACE⁺ and ACE2/TMPRSS2⁺ cells (Figure 5a). Importantly, LA treatment blocked the entry of the D614G mutant virus with IC₅₀ of 2.02 and 2.99 μ M in ACE2⁺ and ACE2/TMPRSS2⁺ cells respectively (Figure 5b), which were comparable to those of the WT virus (Figure 2a and 2b), indicating that LA effectively inhibits SARS-CoV-2 infection regardless of S mutation.

LA possesses a broad spectrum of inhibitory activity against SARS-CoV-2 variants

We then sought to investigate whether LA has the ability to inhibit SARS-CoV-2 variants by imaging SARS-CoV-2 N protein in Vero cells 24 h after the inoculation of authentic virus. The results showed that LA treatment impeded the infection of SARS-CoV-2 variants including Alpha, Beta, Delta, and Omicron with similar IC₅₀ values of 3.37, 3.12, 2.23, and 2.45 μ M, respectively (Figure 6a). Importantly, these values are comparable to that of ancestral virus (IC₅₀: 2.62 μ M) (Figure 2d), providing further corroborating evidence that LA can effectively hinder the infection of SARS-CoV-2, regardless of the types of S-mutation. Of note, remdesivir exhibited less effective and variable inhibitory activity toward SARS-CoV-2 variants (IC₅₀: 4.06 ~ 7.40 μ M) compared to LA (Figure 6b). Together, these results demonstrate that LA blocks the infection of SARS-CoV-2 variants as well as their ancestral virus with similar efficiency and thus implicate that LA can be a broad-spectrum antiviral agent, providing additional protection strategy against infection by SARS-CoV-2 variants

Discussion

Since the outbreak of the COVID-19 pandemic, numerous single herbs and herbal formulations as well as single compounds isolated from the herbal extracts have been reported to exhibit significant anti-SARS-CoV-2 effects through the inhibition of SARS-CoV-2 life cycle by targeting viral proteins such as 3CLpro, PLpro, RNA-dependent RNA polymerase (RdRp), and S protein, and cellular proteins such as ACE2, cathepsin L, and TMPRSS2 (Adeleye et al., 2022; Benarba & Pandiella, 2020; Lee, Park & Cho, 2022). Saponins including triterpenoid saponins derived from various medicinal plants have also been investigated for their therapeutic potential against SARS-CoV-2 (Ebob, Babiaka & Ntie-Kang, 2021). But, most are based on *in silico* studies (Diniz, Perez-Castillo, Elshabrawy, Filho & de Sousa, 2021; Falade, Adelusi, Adedotun, Abdul-Hammed, Lawal & Agboluaje, 2021; Sinha et al., 2021; Yang et al., 2020) and it is only recently that their inhibitory activities have been demonstrated using pseudotyped or authentic SARS-CoV-2. Licorice-saponin A3, a triterpenoid saponin isolated from licorice, was reported to inhibit SARS-CoV-2 by targeting the NSP7, a core component of RdRp (Yi et al., 2022). Hui and co-workers very recently showed that 3-O- β -chacotriosyl ursolic acid saponins they synthesized displays anti-SARS-CoV-2 activity by binding to S protein (Li et al., 2022). However, to our knowledge, there have been few studies verifying the role of natural triterpenoid saponins in preventing SARS-CoV-2 infection at the stage of membrane fusion. We previously reported that PD, a triterpenoid saponin derived from PG, inhibits SARS-CoV-2 infection and proposed the blockade of membrane fusion as a possible mechanism of action by demonstrating its ability to inhibit a well-known membrane fusion event of spontaneous inhibitory postsynaptic currents in acute brain slices (Kim et al., 2021). Here, we discovered that LA, a triterpenoid saponin isolated from CL and has a very similar chemical composition to PD, exhibits inhibitory activity against SARS-CoV-2. To provide direct evidence that LA blocks the membrane fusion mediated by S protein of SARS-CoV-2, we established cell fusion assay systems based on S protein-ACE2 interaction. The results from these assays revealed that LA indeed hinders the S-mediated membrane fusion event, thereby preventing SARS-CoV-2 infection.

Cholesterol is an essential component of cell membranes involved in virus-host cell fusion and cell-cell fusion for SARS-CoV-2 entry and pathological syncytia formation (Barrantes, 2022; Sanders et al., 2021). Thus,

cholesterol-targeting therapeutics have been proposed for the treatment of COVID-19 (Palacios-Rápalo et al., 2021). The role of membrane cholesterol in SARS-CoV-2 infection was highlighted by recent studies showing that 25-hydroxycholesterol inhibits SARS-CoV-2 entry by blocking membrane fusion through depleting accessible cholesterol from plasma membrane (Wang et al., 2020; Zang et al., 2020; Zu et al., 2020). It was also reported that exogenously added 27-hydroxycholesterol accumulates in the plasma membrane lipid rafts, leading to inhibition of SARS-CoV-2 entry (Marcello et al., 2020; Palacios-Rápalo et al., 2021). Together, these studies suggest that transient changes in cholesterol distribution in plasma membranes can exert inhibitory effects on membrane fusion and viral entry. In this regard, we investigated the effects of LA on membrane cholesterol and observed that upon treatment with LA, cholesterol levels at the plasma membrane were significantly increased, implying that LA blocks S-mediated membrane fusion by altering cholesterol distribution in plasma membranes.

In this study, we also explained the structure-activity relationship by comparing the antiviral activity of three different triterpenoid saponins isolated from CL such as LA, LB, and LD. These compounds share structure similarities consisting of 30-carbon triterpene backbone with a single sugar at position C3 and an oligosaccharide chain attached at position C28, but the number of sugar units and the presence or absence of a branched sugar in the oligosaccharide chain are different each other (Figure 1c). Both pSARS-CoV-2 entry assay and cell-to-cell fusion assay identically demonstrated that LA consisting of linearly linked four sugar residues exhibited the most potent antiviral activity compared to LB and LD that are composed of a branched and/or a shorter chain of sugar residues, indicating that both length and linearity of the conjugated sugar residues of triterpenoid saponins are critical for such inhibitory actions. Previously, our molecular modeling studies predicted that triterpene backbone of PD are embedded in the lipid bilayer membrane with an oligosaccharide chain sticking out of the membrane, highlighting the importance of glycosylated group attached at C28 position in the antiviral activity. Thus, the present study corroborates our previous results, further supporting the idea that the linear sugar residues of triterpenoid saponins create a protrusion from the cell membrane and play critical roles in hindering membrane fusion events. Intriguingly, the potency of LA, LB, and LD against SARS-CoV-2 is well correlated with their ability to increase membrane cholesterol levels (Figure 1d, 3d, and S3), raising an interesting possibility that the attached oligosaccharide chain of LA might also be responsible for the alteration of membrane cholesterol. The more detailed studies of the relationships of structure and mechanism of action of triterpenoid saponins including LA are needed to address this hypothesis.

There are many advantages of membrane fusion blockers over other viral entry inhibitors. Because most reported mutations of SARS-CoV-2 variants are clustered near the RBD of S protein, compounds that bind to ancestral S protein and block its interaction with ACE2 might exhibit reduced inhibitory activity against SARS-CoV-2 variants as monoclonal antibodies targeting the RBD of the S protein of ancestral virus showed reduced neutralizing activity against new variants of SARS-CoV-2 (Bekliz et al., 2022; Takashita et al., 2022). Moreover, SARS-CoV-2 entry inhibitors that specifically act on the interaction between S protein and ACE2 do not provide cross-reactivity to other coronaviruses that recognize different cellular receptors, such as MERS-CoV that uses the receptor dipeptidyl peptidase 4 (DPP4) (Mou, Raj, van Kuppeveld, Rottier, Haagmans & Bosch, 2013) and novel enveloped viruses that might utilize a different cellular receptor to enter host cells. In contrast, viral membrane fusion blockers have a broader application since the membrane fusion process is shared in all enveloped viruses including SARS-CoV-2 and its variants. Supporting this notion, we here demonstrated that LA effectively inhibits the infection of the ancestral SARS-CoV-2 and its variants including Omicron with similar IC_{50} values ranging from 2.23 to 3.37 μ M. Another advantage is that, since the membrane fusion is a common event in the virial entry pathways, fusion blockers can prevent two main SARS-CoV-2 entry routes with a similar efficiency. In agreement with this hypothesis, we found that LA inhibits the cell surface and endosomal pathways of SARS-CoV-2 entry with similar IC_{50} values in experiments using pseudotyped and authentic viruses (Figure 2f).

The S-mediated membrane fusion is critical, not only for SARS-CoV-2 entry into host cells but also for syncytia formation. The important roles of syncytia formation in SARS-CoV-2 infection include evasion from neutralizing antibodies and viral spread by cell-to-cell transmission (Rajah, Bernier, Buchrieser &

Schwartz, 2021; Zeng et al., 2022). Moreover, syncytia can lead to cell death via apoptosis or pyroptosis, releasing virus particles to re-infect neighboring cells and triggering an inflammatory response (Sanders et al., 2021; Santana et al., 2021). Here, we observed that LA effectively inhibits S protein-mediated syncytia formation and cellular apoptosis, indicating that LA is able to block SARS-CoV-2 pathological effects. Overall, LA is a natural viral fusion blocker that effectively prevents SARS-CoV-2 and all newly emerging variants from infecting host cells and syncytia formation by hindering the S-mediated membrane fusion. We propose here that LA can be a broad-spectrum antiviral drug not only against SARS-CoV-2 but also against other novel enveloped viral pathogens that might arise in the future.

Author contributions: Conceptualization, T.Y.K., D.S.J., S.K., and C.J.L.; Experimental execution, T.Y.K., S.J., M.K., Y.E.D, and S.-R.S. Methodology and formal analysis, T.Y.K., S.J.; writing-original draft preparation, T.Y.K and S.J.; writing-review and editing, T.Y.K., D.S.J., S.K., and C.J.L. All authors have read and agreed to the published version of the manuscript.

Funding: This work was supported by the Institute for Basic Science (IBS), Center for Cognition and Sociality (IBS-R001-D2) to C.J.L., National Research Foundation of Korea (NRF) with grants funded by the Korean government (MSIT) (NRF-2017M3A9G6068245 to S.K. and NRF-2019R1A2C1083945 to D.S.J.).

Data Availability Statement: Materials are available upon a reasonable request from the corresponding author

Acknowledgement: We appreciate Mr. Chan-yong Kwak for providing the root of *Codonopsis lanceolata* , which motivated the present study. We also thank Haejin Jung and Ph.D. Taek Seung Kim, senior engineers at the Research Solution Center (RSC) in IBS, for performing the flow cytometry analysis and imaging cell-to-cell fusion using Leica DMI8 microscope, respectively.

Conflict of interest s: The authors declare no conflict of interests.

Reference

Adeleye OA, Bamiro OA, Bakre LG, Odeleye FO, Adebowale MN, Okunye OL, *et al.* (2022). Medicinal Plants with Potential Inhibitory Bioactive Compounds against Coronaviruses. *Adv Pharm Bull* 12: 7-16.

Aleem A, Akbar Samad AB, & Slenker AK (2022). Emerging Variants of SARS-CoV-2 And Novel Therapeutics Against Coronavirus (COVID-19). In *StatPearls*. StatPearls Publishing

Copyright © 2022, StatPearls Publishing LLC.: Treasure Island (FL).

Barrantes FJ (2022). The constellation of cholesterol-dependent processes associated with SARS-CoV-2 infection. *Prog Lipid Res* 87: 101166.

Bekliz M, Adea K, Vetter P, Eberhardt CS, Hosszu-Fellous K, Vu DL, *et al.* (2022). Neutralization capacity of antibodies elicited through homologous or heterologous infection or vaccination against SARS-CoV-2 VOCs. *Nat Commun* 13: 3840.

Benarba B, & Pandiella A (2020). Medicinal Plants as Sources of Active Molecules Against COVID-19. *Front Pharmacol* 11: 1189.

Biswas S, Mahmud S, Mita MA, Afrose S, Hasan MR, Paul GK, *et al.* (2022). The Emergence of SARS-CoV-2 Variants With a Lower Antibody Response: A Genomic and Clinical Perspective. *Front Med (Lausanne)* 9: 825245.

Buchrieser J, Dufloo J, Hubert M, Monel B, Planas D, Rajah MM, *et al.* (2020). Syncytia formation by SARS-CoV-2-infected cells. *EMBO J* 39: e106267.

Buchrieser J, Dufloo J, Hubert M, Monel B, Planas D, Rajah MM, *et al.* (2021). Syncytia formation by SARS-CoV-2-infected cells. *EMBO J* 40: e107405.

- Bussani R, Schneider E, Zentilin L, Collesi C, Ali H, Braga L, *et al.* (2020). Persistence of viral RNA, pneumocyte syncytia and thrombosis are hallmarks of advanced COVID-19 pathology. *EBioMedicine* 61: 103104.
- Chen KK, Tsung-Ning Huang D, & Huang LM (2022). SARS-CoV-2 variants - Evolution, spike protein, and vaccines. *Biomed J.*
- Choi JH, Hwang YP, Lee HS, & Jeong HG (2009). Inhibitory effect of Platycodi Radix on ovalbumin-induced airway inflammation in a murine model of asthma. *Food Chem Toxicol* 47: 1272-1279.
- Crawford KHD, Eguia R, Dingens AS, Loes AN, Malone KD, Wolf CR, *et al.* (2020). Protocol and Reagents for Pseudotyping Lentiviral Particles with SARS-CoV-2 Spike Protein for Neutralization Assays. *Viruses* 12.
- de Vries RD, Schmitz KS, Bovier FT, Predella C, Khao J, Noack D, *et al.* (2021). Intranasal fusion inhibitory lipopeptide prevents direct-contact SARS-CoV-2 transmission in ferrets. *Science* 371: 1379-1382.
- DeGrace MM, Ghedin E, Frieman MB, Krammer F, Grifoni A, Alisoltani A, *et al.* (2022). Defining the risk of SARS-CoV-2 variants on immune protection. *Nature* 605:640-652.
- Diniz LRL, Perez-Castillo Y, Elshabrawy HA, Filho C, & de Sousa DP (2021). Bioactive Terpenes and Their Derivatives as Potential SARS-CoV-2 Proteases Inhibitors from Molecular Modeling Studies. *Biomolecules* 11.
- Du YE, Lee JS, Kim HM, Ahn JH, Jung IH, Ryu JH, *et al.* (2018). Chemical constituents of the roots of *Codonopsis lanceolata*. *Arch Pharm Res* 41: 1082-1091.
- Du Z, Hong H, Wang S, Ma L, Liu C, Bai Y, *et al.* (2022). Reproduction Number of the Omicron Variant Triples That of the Delta Variant. *Viruses* 14.
- Ebob OT, Babiaka SB, & Ntie-Kang F (2021). Natural Products as Potential Lead Compounds for Drug Discovery Against SARS-CoV-2. *Nat Prod Bioprospect* 11: 611-628.
- Falade VA, Adelusi TI, Adedotun IO, Abdul-Hammed M, Lawal TA, & Agboluaje SA (2021). In silico investigation of saponins and tannins as potential inhibitors of SARS-CoV-2 main protease (M(pro)). *In Silico Pharmacol* 9: 9.
- Gowrisankar A, Priyanka TMC, & Banerjee S (2022). Omicron: a mysterious variant of concern. *Eur Phys J Plus* 137: 100.
- Hoffmann M, Kleine-Weber H, Schroeder S, Krüger N, Herrler T, Erichsen S, *et al.* (2020). SARS-CoV-2 Cell Entry Depends on ACE2 and TMPRSS2 and Is Blocked by a Clinically Proven Protease Inhibitor. *Cell* 181: 271-280.e278.
- Hoffmann M, Krüger N, Schulz S, Cossmann A, Rocha C, Kempf A, *et al.* (2022). The Omicron variant is highly resistant against antibody-mediated neutralization: Implications for control of the COVID-19 pandemic. *Cell* 185:447-456.e411.
- Hooper P, Zaki S, Daniels P, & Middleton D (2001). Comparative pathology of the diseases caused by Hendra and Nipah viruses. *Microbes Infect* 3: 315-322.
- Hossen MJ, Kim MY, Kim JH, & Cho JY (2016). *Codonopsis lanceolata*: A Review of Its Therapeutic Potentials. *Phytother Res* 30: 347-356.
- Huang Y, Yang C, Xu XF, Xu W, & Liu SW (2020). Structural and functional properties of SARS-CoV-2 spike protein: potential antiviral drug development for COVID-19. *Acta Pharmacol Sin* 41: 1141-1149.
- Kim TY, Jeon S, Jang Y, Gotina L, Won J, Ju YH, *et al.* (2021). Platycodin D, a natural component of *Platycodon grandiflorum*, prevents both lysosome- and TMPRSS2-driven SARS-CoV-2 infection by hindering membrane fusion. *Exp Mol Med* 53: 956-972.

- Lee M, Park J, & Cho IH (2022). Target-Specific Drug Discovery of Natural Products against SARS-CoV-2 Life Cycle and Cytokine Storm in COVID-19. *Am J Chin Med* 50:927-959.
- Lee S, Han EH, Lim MK, Lee SH, Yu HJ, Lim YH, *et al.* (2020). Fermented *Platycodon grandiflorum* Extracts Relieve Airway Inflammation and Cough Reflex Sensitivity In Vivo. *J Med Food* 23: 1060-1069.
- Li H, Cheng C, Shi S, Wu Y, Gao Y, Liu Z, *et al.* (2022). Identification, optimization, and biological evaluation of 3-O- β -chacotriosyl ursolic acid derivatives as novel SARS-CoV-2 entry inhibitors by targeting the prefusion state of spike protein. *Eur J Med Chem* 238: 114426.
- Liu S, Xiao G, Chen Y, He Y, Niu J, Escalante CR, *et al.* (2004). Interaction between heptad repeat 1 and 2 regions in spike protein of SARS-associated coronavirus: implications for virus fusogenic mechanism and identification of fusion inhibitors. *Lancet* 363: 938-947.
- Lu L, Liu Q, Zhu Y, Chan KH, Qin L, Li Y, *et al.* (2014). Structure-based discovery of Middle East respiratory syndrome coronavirus fusion inhibitor. *Nat Commun* 5: 3067.
- Marcello A, Civra A, Milan Bonotto R, Nascimento Alves L, Rajasekharan S, Giacobone C, *et al.* (2020). The cholesterol metabolite 27-hydroxycholesterol inhibits SARS-CoV-2 and is markedly decreased in COVID-19 patients. *Redox Biol* 36:101682.
- Mou H, Raj VS, van Kuppeveld FJ, Rottier PJ, Haagmans BL, & Bosch BJ (2013). The receptor binding domain of the new Middle East respiratory syndrome coronavirus maps to a 231-residue region in the spike protein that efficiently elicits neutralizing antibodies. *J Virol* 87: 9379-9383.
- Nardacci R, Perfettini JL, Grieco L, Thieffry D, Kroemer G, & Piacentini M (2015). Syncytial apoptosis signaling network induced by the HIV-1 envelope glycoprotein complex: an overview. *Cell Death Dis* 6: e1846.
- Newman DJ, & Cragg GM (2020). Natural Products as Sources of New Drugs over the Nearly Four Decades from 01/1981 to 09/2019. *J Nat Prod* 83: 770-803.
- Ozono S, Zhang Y, Ode H, Sano K, Tan TS, Imai K, *et al.* (2021). SARS-CoV-2 D614G spike mutation increases entry efficiency with enhanced ACE2-binding affinity. *Nat Commun* 12: 848.
- Palacios-Rápalo SN, De Jesús-González LA, Cordero-Rivera CD, Farfan-Morales CN, Osuna-Ramos JF, Martínez-Mier G, *et al.* (2021). Cholesterol-Rich Lipid Rafts as Platforms for SARS-CoV-2 Entry. *Front Immunol* 12: 796855.
- Rahmani S, & Rezaei N (2022). Omicron (B.1.1.529) variant: Development, dissemination, and dominance. *J Med Virol* 94: 1787-1788.
- Rajah MM, Bernier A, Buchrieser J, & Schwartz O (2021). The Mechanism and Consequences of SARS-CoV-2 Spike-Mediated Fusion and Syncytia Formation. *J Mol Biol*:167280.
- Rihn SJ, Merits A, Bakshi S, Turnbull ML, Wickenhagen A, Alexander AJT, *et al.* (2021). A plasmid DNA-launched SARS-CoV-2 reverse genetics system and coronavirus toolkit for COVID-19 research. *PLoS Biol* 19: e3001091.
- Sanders DW, Jumper CC, Ackerman PJ, Bracha D, Donlic A, Kim H, *et al.* (2021). SARS-CoV-2 requires cholesterol for viral entry and pathological syncytia formation. *Elife* 10.
- Santana MF, Pinto RAA, Marcon BH, Medeiros L, Morais T, Dias LC, *et al.* (2021). Pathological findings and morphologic correlation of the lungs of autopsied patients with SARS-CoV-2 infection in the Brazilian Amazon using transmission electron microscopy. *Rev Soc Bras Med Trop* 54: e0850.
- Schrors B, Riesgo-Ferreiro P, Sorn P, Gudimella R, Bukur T, Rosler T, *et al.* (2021). Large-scale analysis of SARS-CoV-2 spike-glycoprotein mutants demonstrates the need for continuous screening of virus isolates. *PLoS One* 16:e0249254.

- Scovino AM, Dahab EC, Vieira GF, Freire-de-Lima L, Freire-de-Lima CG, & Morrot A (2022). SARS-CoV-2's Variants of Concern: A Brief Characterization. *Front Immunol* 13: 834098.
- Seo YS, Kim HS, Lee AY, Chun JM, Kim SB, Moon BC, *et al.* (2019). *Codonopsis lanceolata* attenuates allergic lung inflammation by inhibiting Th2 cell activation and augmenting mitochondrial ROS dismutase (SOD2) expression. *Sci Rep* 9: 2312.
- Sinha SK, Shakya A, Prasad SK, Singh S, Gurav NS, Prasad RS, *et al.* (2021). An in-silico evaluation of different Saikosaponins for their potency against SARS-CoV-2 using NSP15 and fusion spike glycoprotein as targets. *J Biomol Struct Dyn* 39: 3244-3255.
- Takashita E, Kinoshita N, Yamayoshi S, Sakai-Tagawa Y, Fujisaki S, Ito M, *et al.* (2022). Efficacy of Antibodies and Antiviral Drugs against Covid-19 Omicron Variant. *N Engl J Med* 386: 995-998.
- Tang T, Bidon M, Jaimes JA, Whittaker GR, & Daniel S (2020). Coronavirus membrane fusion mechanism offers a potential target for antiviral development. *Antiviral Res* 178:104792.
- Wang S, Li W, Hui H, Tiwari SK, Zhang Q, Croker BA, *et al.* (2020). Cholesterol 25-Hydroxylase inhibits SARS-CoV-2 and other coronaviruses by depleting membrane cholesterol. *Embo j* 39: e106057.
- Xia S, Liu M, Wang C, Xu W, Lan Q, Feng S, *et al.* (2020). Inhibition of SARS-CoV-2 (previously 2019-nCoV) infection by a highly potent pan-coronavirus fusion inhibitor targeting its spike protein that harbors a high capacity to mediate membrane fusion. *Cell Res* 30: 343-355.
- Xia S, Yan L, Xu W, Agrawal AS, Algaissi A, Tseng CK, *et al.* (2019). A pan-coronavirus fusion inhibitor targeting the HR1 domain of human coronavirus spike. *Sci Adv* 5: eaav4580.
- Yang R, Liu H, Bai C, Wang Y, Zhang X, Guo R, *et al.* (2020). Chemical composition and pharmacological mechanism of Qingfei Paidu Decoction and Ma Xing Shi Gan Decoction against Coronavirus Disease 2019 (COVID-19): In silico and experimental study. *Pharmacol Res* 157: 104820.
- Yi Y, Li J, Lai X, Zhang M, Kuang Y, Bao YO, *et al.* (2022). Natural triterpenoids from licorice potentially inhibit SARS-CoV-2 infection. *J Adv Res* 36: 201-210.
- Zaman R, Orakzai SA, & Yunus A (1987). Effect of pyrazinamide on serum and urinary uric acid levels. *J Pak Med Assoc* 37: 76-78.
- Zang R, Case JB, Yutuc E, Ma X, Shen S, Gomez Castro MF, *et al.* (2020). Cholesterol 25-hydroxylase suppresses SARS-CoV-2 replication by blocking membrane fusion. *Proc Natl Acad Sci U S A* 117: 32105-32113.
- Zeng C, Evans JP, King T, Zheng YM, Oltz EM, Whelan SPJ, *et al.* (2022). SARS-CoV-2 spreads through cell-to-cell transmission. *Proc Natl Acad Sci U S A* 119.
- Zhang L, Jackson CB, Mou H, Ojha A, Peng H, Quinlan BD, *et al.* (2020). SARS-CoV-2 spike-protein D614G mutation increases virion spike density and infectivity. *Nat Commun* 11: 6013.
- Zu S, Deng YQ, Zhou C, Li J, Li L, Chen Q, *et al.* (2020). 25-Hydroxycholesterol is a potent SARS-CoV-2 inhibitor. *Cell Res* 30: 1043-1045.

Figure Legends

FIGURE 1 *Codonopsis lanceolata* extract and lancemaside A inhibit SARS-CoV-2 infection. (a,b) The effects of 70% EtOH extracts from the aerial parts and roots of *Codonopsis lanceolata* (CL) on the entry of SARS-CoV-2 pseudovirus into ACE2⁺ H1299 cells (a) and the viability of H1299 cells (b). (c) The chemical structures of tangshenoside I (1), ethylsyringin (2), syringin (3), sinapaldehyde glucoside (4), lobetyolin (5), lancemasides A (6), B (7), and D (8) obtained from the roots of CL. (d) pSARS-CoV-2 entry assay with eight compounds described in (c) in ACE2⁺ and ACE2/TMPRSS2⁺ H1299 cells.

FIGURE 2 Lancemaside A inhibits both endocytic and TMPRSS2-mediated SARS-CoV-2 entry pathways. (a-c) The effects of LA on the entry of SARS-CoV-2 pseudovirus (pSARS-CoV-2) into ACE2⁺ (a) and ACE2/TMPRSS2⁺ (b) H1299 cells, and H1299 cell viability (c). The data were representative of three independent experiments with triplicate samples. The error bars indicate the SEM. (d,e) Dose-response curves and confocal images of SARS-CoV-2 N protein (green) and cell nuclei (red) for LA (d) and remdesivir (e) on the infection of ancestral SARS-CoV-2 (black circle) in Vero cells. The blue squares represent Vero cell viability. F Dose-response curve for LA against SARS-CoV-2 recombinant viruses expressing nanoluciferase (Nluc) into A549 cells overexpressing both ACE2 and TMPRSS2. The blue square represents cell viability. The mean \pm SEM was calculated from duplicate experiments.

FIGURE 3 Lancemaside A blocks SARS-CoV-2 S-mediated membrane fusion. (a) Schematics for SARS-CoV-2 Spike-ACE2 binding assay using S-RBD-GFP, a recombinant protein comprised of receptor binding domain (RBD) of S protein fused to GFP and ACE2⁺H1299 cells. (b) The effect of CL extracts and LA on the binding of S-RBD-GFP to ACE2 overexpressed on the surface of H1299 cells was determined by flow cytometry after pretreatment with indicated concentration of CL extracts and LA. The grey peaks indicate the control experiments without S-RBD-GFP addition. The same control data were used for each flow cytometry graphs. (c, d) The effect of LA on membrane fusion between Spike-HEK293 (EGFP⁺) and ACE2/TMPRSS2⁺-H1299 (mRuby2⁺) cells was monitored by time-lapse microscopy (c), and determined by counting the number of EGFP/mRuby2 double positive cells by flow cytometry (d). EGFP⁺ HEK293 cells (no spike) were used for control experiment. All compounds were used at the concentration of 10 μ M. The data were representative of three independent experiments. (c). (f, g) Filipin staining of intracellular cholesterol in ACE2⁺H1299 and parental H1299 cells after treatment with DMSO or 10 μ M LA for 1 h (f) and quantification of the membrane cholesterol levels using Image J (n = 14 for each group). Error bars in the graphs indicate the SEM. P values were determined by the unpaired, two-tailed Student's t-test. ****P < 0.0001 (g).

FIGURE 4 Lancemaside A inhibits S-mediated syncytia formation. (a) Schematic diagram of the Split-GFP assay to monitor syncytia formation. (b) Experimental timeline for the split-GFP fusion assay. (c) GFP and DAPI (blue) fluorescent images indicate syncytia formed by cell-to-cell fusion and cell nuclei, respectively (upper panel). DAPI nuclear staining overlapped and non-overlapped with GFP fluorescence are pseudocolored in green and red, respectively (lower panel). (d) Quantitative assessment of syncytia formation. GFP and DAPI images were obtained in three random fields per well and the percentage of syncytia formation were calculated by dividing number of nuclei in GFP-positive cells by total number of nuclei. The data were representative of three independent experiments. The error bars indicate the SEM. P values were determined by ANOVA followed by Tukey's post hoc test. ****P < 0.0001; NS not significant. (e) Western blot analysis using protein lysates from split-GFP experiments (incubation time was 72 h) with anti-cleaved caspase-3 and -9 antibodies. GAPDH was used as a loading control.

FIGURE 5 Lancemaside A inhibits the infection of SARS-CoV-2 WT and D614G mutant. (a) The infection levels of WT and D614G mutant of pSARS-CoV-2 in ACE2⁺ and ACE2/TMPRSS2⁺ H1299 cells. P values were determined by the unpaired, two-tailed Student's t-test (****P < 0.0001). (b) The effects of LA on the infection of WT and D614G mutant of pSARS-CoV-2 in ACE2⁺ and ACE2/TMPRSS2⁺ H1299 cells. The data from pSARS-CoV-2 entry assay were representative of three independent experiments with triplicate samples. The error bars indicate the SEM.

FIGURE 6 Lancemaside A effectively inhibits the infection of SARS-CoV-2 variants (a,b) Dose-response curves for LA (a) and remdesivir (b) against various SARS-CoV-2 variants including Alpha (B.1.1.7), Beta (B.1.351), Delta (B.1.617.2), and Omicron (B.1.1.529) in Vero cells. The mean \pm SEM was calculated from duplicate experiments. Confocal images of SARS-CoV-2 N protein (green) and cell nuclei (red) at concentrations near the IC₅₀ of LA.

Figure 2

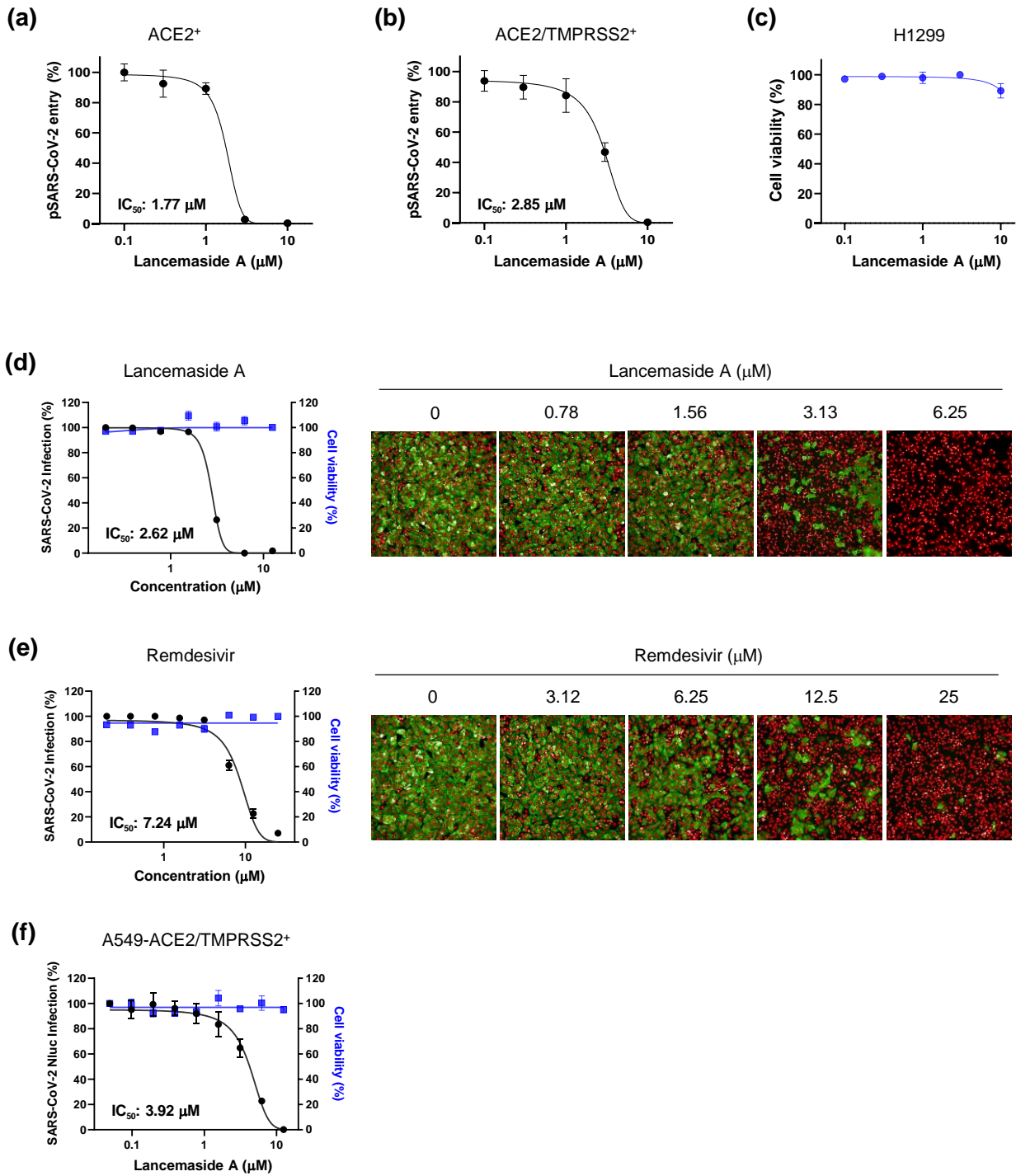


Figure 3

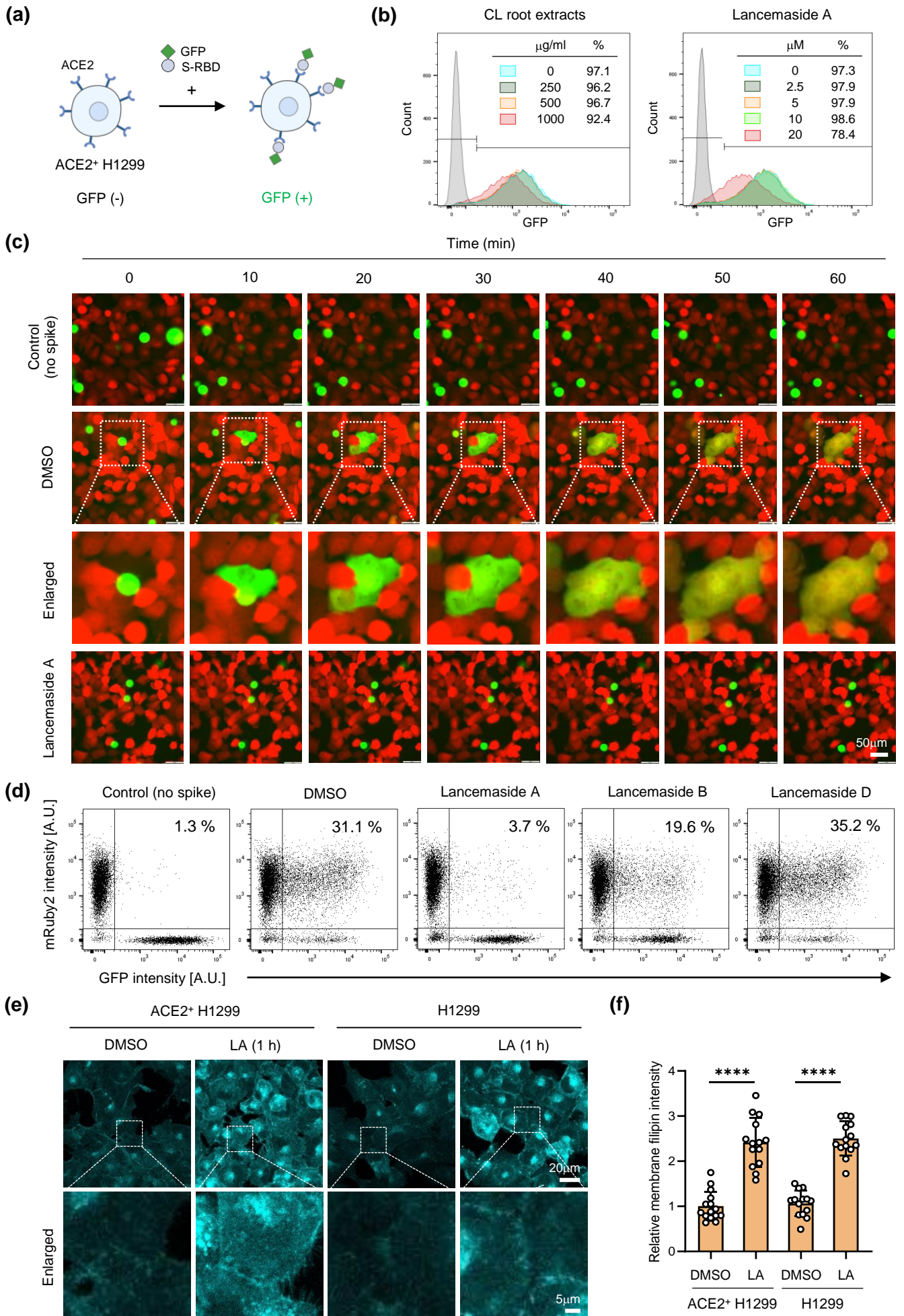
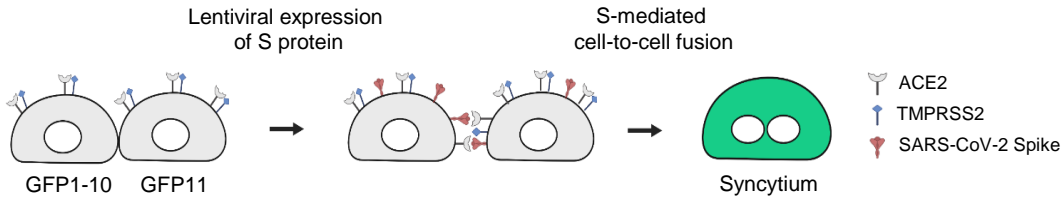
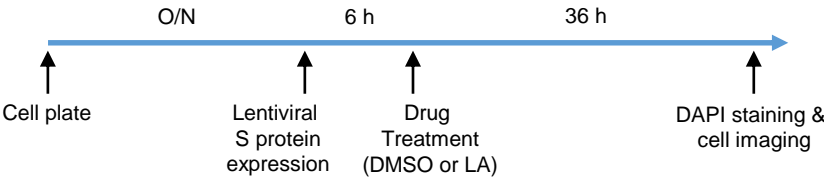


Figure 4

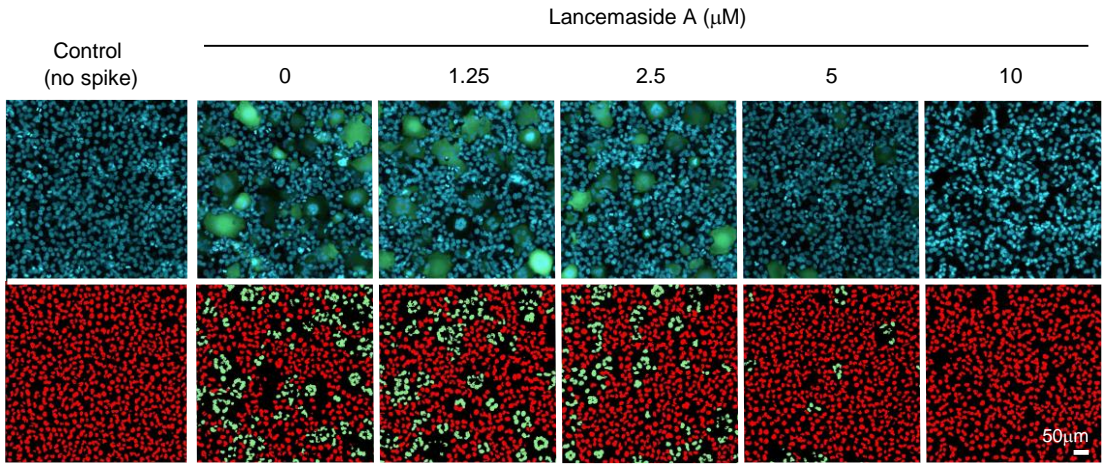
(a)



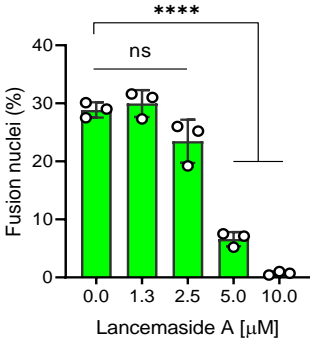
(b)



(c)



(d)



(e)

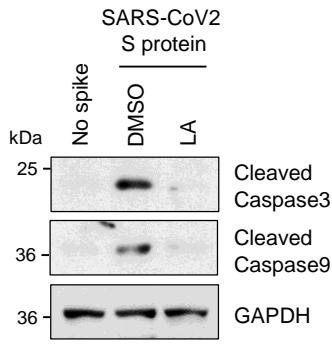
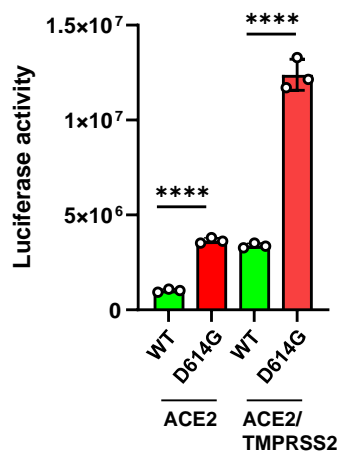


Figure 5

(a)



(b)

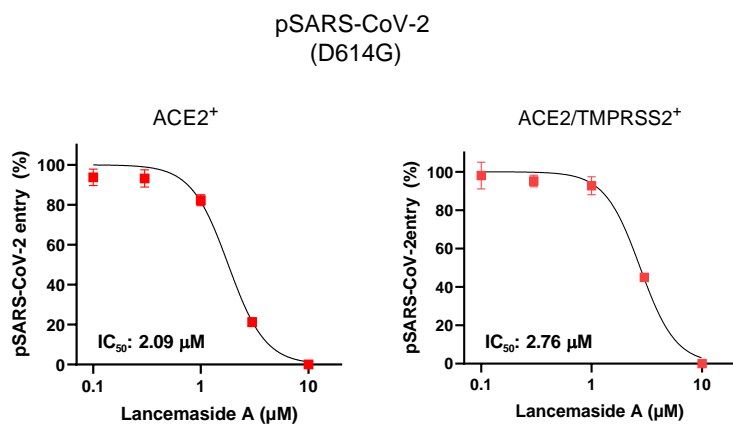
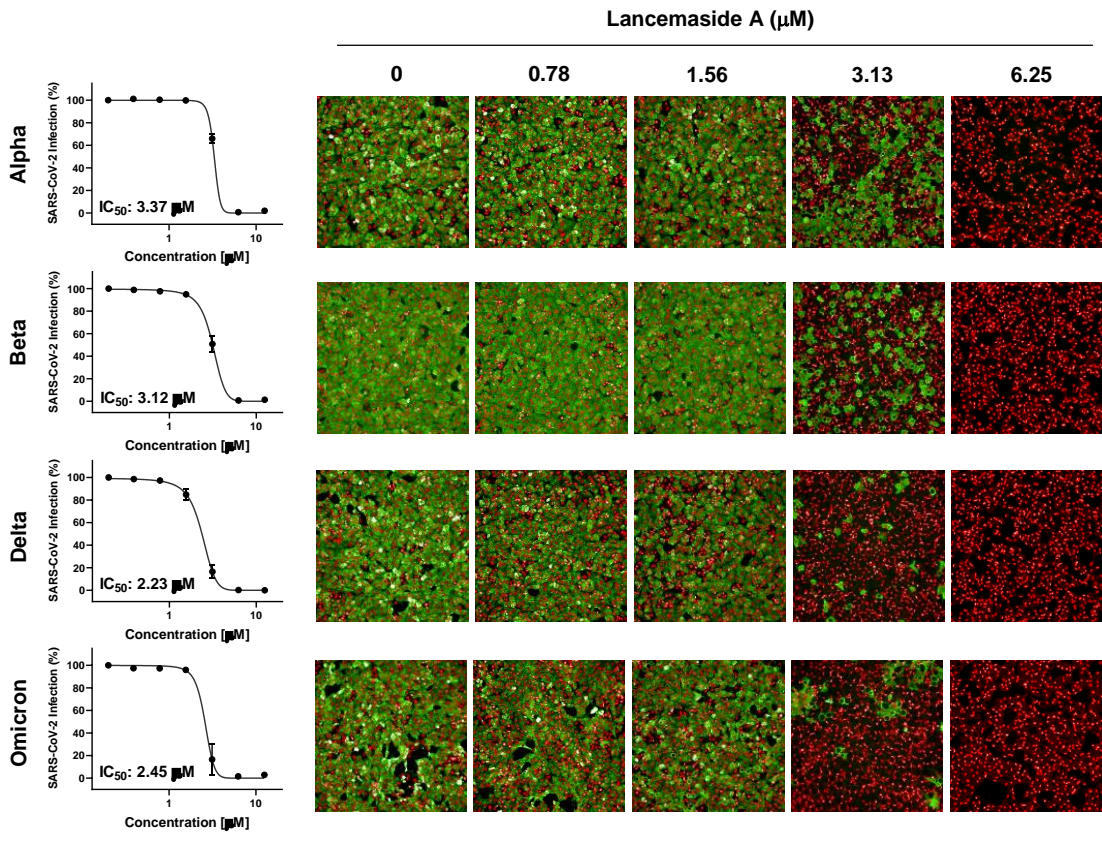


Figure 6

(a)

SARS-CoV-2 variants



(b)

SARS-CoV-2 variants

